Nanocrystalline precipitates formed by aging of bcc disordered Fe-Ni-Mo alloys

C. Djega-Mariadassou
Laboratoire de Structure des Matériaux Métalliques, Université de Paris-Sud, Bâtiment 414, 91405 Orsay Cedex, France

L. Bessais*
Groupe de Physique des Solides Paris7 et Paris6, Tour 23, 2 place Jussieu, 75251 Paris CEDEX 05, France

C. Servant
Laboratoire de Métallurgie Structurale, Université de Paris-Sud, Bâtiment 414, 91405 Orsay Cedex, France
(Received 10 December 1993; revised manuscript received 10 November 1994)

A quantitative analysis of the ^{57}Fe hyperfine field distribution $P(H)$ has been performed in quenched bcc disordered Fe-Ni-M allows (M=W,Mo) in order to determine the matrix depletion of Ni and Mo atoms that occurs after aging. $P(H)$ has been described as the result of the convolution of the distribution given by the multinomial law applied to the two first coordination shells of Fe nuclei and a Gaussian function the variance of which affects the upper shells. The small atomic fraction assigned to the precipitates, observed on the Mössbauer spectra after a 72-h aging at 450 °C of $Fe_{78.3}Ni_{18.3}Mo_{3.4}$ and $Fe_{79.3}Ni_{15.0}Mo_{5.7}$ alloys, is corroborated by the small volume fraction of the nanocrystalline precipitates revealed by transmission electron microscopy (TEM). The two precipitated phases [$(Fe\text{-}Ni)_3Mo$ and $\omega(Fe\text{-}Ni)_7Mo_2$] detected by TEM are consistent with the Mössbauer approach, with an overall Fe to (Ni,Mo) atomic ratio twice smaller for $Fe_{79.3}Ni_{15.0}Mo_{5.7}$ than for $Fe_{78.3}Ni_{18.3}Mo_{3.4}$, giving evidence for an evolution to depleted-Fe species.

I. INTRODUCTION

The maraging (martensite-aged phase) family consists of a bcc lattice mainly of Fe, Ni, and/or Co with additional elements, providing after thermal treatment the precipitation of intermetallic compounds responsible for their interesting mechanical properties. The difficulty for analysis is in the particularly ultrafine scale of the microstructure (some 10 nm) so that the subject is still open. Experimentally, information about the alloy modifications is usually obtained from electron microscopy, atom probe,[1] or from small-angle x-ray or neutron scattering.[2] For these last techniques, full information results from complex procedures. Consequently, we think that Mössabuer spectroscopy, more easy to implement, could be, within constraints and limitations to be outlined, a reliable approach to the structural analysis of these materials, provided that comparison with other techniques can be made. The choice of the Fe-Ni-based system was defined by the fact that the trend for Ni is to distribute randomly more easily than Co. Moreover, while W and Mo are known to reduce the Fe magnetic hyperfine field (MHF) drastically, the effect of Ni is weak but opposite. Their combined influence could be a good test to check the reliability of the simple approach assuming the additivity of the solute perturbations.

In a ternary crystalline alloy, the atomic configurations can be described by the specifications of the correlations between pairs of atoms. X-ray diffraction experiments with anomalous scattering can provide information but these are difficult in practice. Mössbauer spectroscopy with ^{57}Co is able to give the iron-metal order parameters more directly and was applied semiquantitatively recently at room temperature to determine the state of order in bcc $Fe_{49}Co_{49}Mo_2$.[3] Two types of short-range order correlations were obtained: the amount of $B2$ order associated with the Fe-Co atom configurations and secondly the correlations between Fe and Mo neighbors. The analysis of the Mo effect was based on a model assuming the additivity of the Fe magnetic hyperfine field perturbations resulting from the solutes in the nearest neighboring lattice sites, as reported in binary-iron-based alloys. The perturbations caused by the first and second Mo neighbors were considered as similar, although differences were observed previously in binary Fe-Mo dilute alloys.[4] The magnetic hyperfine field distribution $P(H)$ was modeled as three Gaussians corresponding, respectively, to Fe atoms without Mo and with one and two Mo neighbors and converted, to simulate the spectra, by convoluting them with a sextet of Lorentzian lines, for comparison with the experimental spectra. The concept of additivity successful for dilute binary alloys was considered by the authors of Ref. 3 to be inadequate for this Fe-Co composition. They based their analysis of the Co effect in terms of changes in conduction electrons and core polarization of the iron atoms, as one of them did previously for nondilute Fe-Ni alloys at low temperature.[5] They argued that, in the case of a magnetic second component, $P(H)$ cannot be parameterized in terms of the number of solute atom perturbations, as developed with nonmagnetic solutes, but rather by the exchange interactions affecting the Fe nuclei. The magnetic hyperfine field was considered as resulting from two components, one proportional to changes in the local magnetic moment at the Fe atoms induced by neighboring solutes and the second corresponding to a transferred MHF arising from the spin

polarization induced by exchange interactions with the spins of neighboring atoms. Allowing the Fe magnetic moment around the magnetic solute to vary with the position of the other nearby solute atoms, the authors of Ref. 3 proceeded to a detailed description of the locations of the magnetic solute atoms in the bcc matrix by Monte Carlo type simulations. The magnetic moments of the atoms in the first three nearest neighbor shells of the Fe atom were calculated by accounting for solute-induced magnetic moment perturbations through their fifth nearest neighbor shell. Such an interpretation derives mainly from high-concentration behavior. If the model was also found suitable for lower Co content, this does not exclude in the lower concentration range the use of additive parameters which, moreover, do not involve prejudgment about the spin polarization influence. Nagy *et al.*[6] generalized the model that assumes the additive and statistical effect of the iron field perturbations in binary alloys with a few percent of substitutional alloying elements to ternary alloys, with higher concentration of the third element. They determined successfully, at room temperature, the atomic Cr concentration in bcc $Fe_{1-x-y}Ni_xCr_y$ alloys ($x \simeq 0.04, y \simeq 0.10$) from analysis of the magnetic hyperfine field distribution. Such an approach is justified, the more especially as the Ni influence is the smallest detected among the solute effects measured in the bcc Fe matrix. An analytical method was elaborated, taking into account three distribution peaks resulting from the binomial law, which were fitted with the three corresponding amplitude peaks of $P(H)$. Fourteen neighbors belonging to the first and second neighboring shell lattice sites were included. The convolution distribution produce of the binomial distribution with a Gaussian function was determined. The decreasing effect of Cr atoms on the Fe hyperfine field was detected at higher field (35.0 kOe) than the value of 26.9 kOe states previously in binary Fe-Cr alloys, but the effect of Ni was not defined accurately.[4] The perspectives given by this approach seem promising although no clear demonstration of the quality of the $P(H)$ fits was provided. The aim of this paper is to reach the atom distribution in the ternary bcc $Fe_{1-x-y}Ni_xM_y$ matrix (M=Mo,W) (with $x \simeq 0.15-0.18, y \simeq 0.03-0.05$) in order to explain the microstructure of aged Fe maraging type alloys. Knowledge of the bcc matrix modifications occurring during aging can provide essential information about the concomitant metastable precipitate formation.

The first part of this work is devoted to a preliminary study of $Fe_{1-x}Ni_x$ binary alloys for the Ni composition range involving that of the $Fe_{1-x-y}Ni_xM_y$(M=Mo,W) ternary alloys which will be explored later on (up to $x=0.18$). In a second step, we define the Ni, W, and Mo perturbations in the ternary disordered alloys with low M concentrations. Lastly, the practical situation of aged alloys with microstructural precipitation is considered.

II. EXPERIMENT

Various $Fe_{1-x}Ni_x$ alloys were made from the low-concentration range $x \simeq 0.03-0.06$ up to higher content to $x \simeq 0.18$, by a sintering process from high-purity powders. The green pellets were annealed at 1200 °C under H_2 atmosphere for 4 h, then co-rolled to 100 μm thick, finally annealed again, and quenched at the rate of 300 °C/h. The same process was carried out for the $Fe_{1-x-y}Ni_xM_y$ (M=Mo,W) alloys but the homogenization temperature was 1400 °C and several annealing and co-rolling cycles were performed. Two cooling rates were selected, 80 °C/s and 300 °C/h, in order to test the cooling rate influence upon the segregation of the additional Mo and W elements. The aging temperature was chosen as 450 °C. The overall atomic composition obtained by x-ray microprobe analysis was homogeneous within the scale of $1\mu m^3$ repeated in numerous areas in the sample.

The Mössbauer spectra were collected at room temperature with a 50 mC ^{57}Co/Rh source in transmission geometry using a constant acceleration 512-channel spectrometer. The parabolic distortion was canceled by working in the mirror image mode and the small resulting linear drift of the baseline was corrected. The sample thickness was chemically reduced to 15 μm in order to eliminate the thickness distortion correction. The α-Fe reference at 290 K had a full width at half maximum of 0.24 mm/s for the external peaks. The experimental data were analyzed by two consecutive procedures. The spectra were first classically decomposed into discrete subspectra using a least squares minimization assuming Lorentzian lines.[7] After various successive fitting steps, the final solution was obtained with all parameters free, providing the isomer shift (δ) and quadrupole splitting (ϵ) correlations as a function of the MHF (H) required for the second procedure. The experimental magnetic hyperfine field distribution $P(H)_{expt}$ was finally extracted from the Mössbauer spectra with the method given by Le Caer and Dubois[8] using an improved version of the Hesse and Rübartsch method with MHF values large compared with the electric quadrupole effect and the linewidth of each elementary site equal to 0.24 mm/s. Transmission electron microscopy (TEM) studies were systematically performed upon the sample previously studied with Mössbauer spectroscopy.

III. CALCULATION OF THE MAGNETIC HYPERFINE FIELD DISTRIBUTION

The MHF experienced by one Fe nucleus belonging to a bcc host lattice with solutes statistically distributed, following the generalization to ternary alloys,[6] is given as

$$H = H_0 + \sum_{i=1}^{2} n_i \Delta H_i \ , \tag{1}$$

where H_0 is the MHF of pure iron, n_i the number of solute neighboring atoms in the coordination sphere i, and ΔH_i the hyperfine field increment corresponding to the ith coordination sphere.

The distribution of the alloying elements around the host iron nucleus is random on the first and second coordination shell i for disordered alloys. The influence of the third coordination sphere and beyond is neglected at this step.

Let p_0 be the atomic proportion of the host iron atom in the alloys and p_k the atomic proportion of the kth al-

loying element, $\sum_{k=0}^{K} p_k = 1$. When the atoms are distributed randomly into the spheres i with $i = 1,2$, the probability P_{α_i} of a given configuration $\alpha_i = \{n_{1,i},\ldots,n_{k,i}\}$ with k varying from 1 to 8 for $i = 1$ and from 1 to 6 for $i = 2$ follows the well known multinomial distribution law

$$P_{\alpha_i} = \frac{N_i!}{\prod_{k=0}^{K} n_{k,i}!} \prod_{k=0}^{K} p_k^{n_{k,i}} , \tag{2}$$

where $N_i = 8$ for $i = 1$ and 6 for $i = 2$. Assuming the independence of the atom distribution in the first two shells, the total probability of the configuration α_i is

$$P_\alpha = \prod_{i=1}^{2} P_{\alpha_i} , \tag{3}$$

α being the combined configuration $\alpha = \{\alpha_1, \alpha_2\}$. The total hyperfine field is then equal to

$$H(\alpha) = H_0 + \sum_{i=1}^{2} \sum_{k=1}^{K} n_{k,i} \Delta H_{k,i} , \tag{4}$$

where $n_{k,i}$ is the number of atoms of species k in sphere i and $\Delta H_{k,i}$ is the corresponding hyperfine field increment.

It would be more realistic to summarize the effects over a higher number of coordination spheres, each one having an influence of smaller magnitude as it becomes more distant from the nucleus. We suggest that these effects can be thought of as random variables of zero mean and finite variance. The law of large numbers dictates that their asymptotic behavior is distribution according to a Gaussian law of zero mean and finite variance $G(0,\sigma)$.

This justifies our assumption that the correct distribution of the hyperfine fields results from the convolution of the distribution given by the multinomial distribution of the two first coordination shells and the Gaussian distribution of the disturbance H_D caused by the more distant shells. Because of the hypothesis of additivity of hyperfine fields, the resulting field on an Fe nucleus is obtained by

$$H = H(\alpha) + H_D , \tag{5}$$

so that the calculated hyperfine field probability $P(H)_c$ is

$$P(H)_c = P(H(\alpha)) \times P(H_D) , \tag{6}$$

where $P(H(\alpha))$ is the probability for a field $H(\alpha)$ in the configuration $\alpha = (\alpha_1, \alpha_2)$ and $P(H_D) = G(0,\sigma)$.

It follows that the adjustable parameters occurring in the $P(H)_c$ calculation are the alloy composition fixing the binomial law, the MHF increments ($\Delta H_{k,i}$) belonging to the alloying element k in the first and second coordination shells, and the variance σ of the Gaussian function affecting the upper shells. However, a realistic evaluation of the experimental ^{57}Fe MHF increments has to take into account the local experimental isomer shift (δ) and quadrupole splitting (ϵ) associated with a particular MHF. The experimental hyperfine field distribution $P(H)_{\text{expt}}$ extracted from the experimental Mössbauer spectra is defined with the δ and ϵ experimental values associated with each individual hyperfine field deduced from the H,δ and H,ϵ correlations resulting from the discrete site analysis procedure. The agreement factor R is expressed as

$$R = \left[\frac{\Sigma_l [P_l(H)_c - P_l(H)_{\text{expt}}]^2}{N} \right]^{1/2} ,$$

where $P_l(H)_c$ and $P_l(H)_{\text{expt}}$ are, respectively, the hyperfine field distribution calculated with the model and the hyperfine field distribution extracted from the experimental data, and N is the number of experimental data. We must emphasize that the minimum R value is directly connected to the solution giving the best agreement between the calculated Mössbauer spectrum and the experimental one, ensuring a direct physical meaning to the two curves $P_l(H)_c$ and $P_l(H)_{\text{expt}}$. For the quenched alloys, the composition values were fixed within the limits given by the x-ray microprobe analysis. (See Table I.) The field increments were adjusted to minimize the agreement factor R by successive steps. The first shell increment being fixed, the second shell increment was varied at each time by various values of σ. For the 72-h-aged samples, the composition was the variable, the field increment parameters being fixed within the limits obtained from the quenched alloys, except for σ which was systematically varied.

TABLE I. Atomic composition from x-ray microanalysis. The accuracy is ±0.002.

Sample	Ni	M
$Fe_{1-x}Ni_x$ (A)	0.178	
$Fe_{1-x}Ni_x$ (B)	0.121	
$Fe_{1-x}Ni_x$ (C)	0.092	
Fe-Ni-W_3 (I)	0.163	0.030
Fe-Ni-Mo_3 (II)	0.183	0.034
Fe-Ni-Mo_5 (III)	0.150	0.057

IV. RESULTS AND DISCUSSION

The field increments $\Delta H_{k,i}$ available up to now are values obtained at room temperature in binary $Fe_{1-x}M_x$ alloys with low M concentrations $x = 0.015$–0.05 for Ni, 0.01 for Mo, and 0.03 and 0.05 for W.[4] These known $\Delta H_{k,i}$ values led in the case of the ternary alloys studied here to a calculated $P(H)_c$ curve significantly shifted to higher field values from the experimental one. Several reasons could be invoked: possibly the failure of the additivity concept for higher Ni content or the disagreement between the field increments measured in binary alloys and those of ternary alloys. We therefore began our study with the MHF distribution analysis of $Fe_{1-x}Ni_x$ alloys before the study of the $Fe_{1-x-y}Ni_xM_y$ alloys in the initial stage precluding the precipitation process. We investigated, afterwards, the aged $Fe_{1-x-y}Ni_xM_y$ alloys during their advanced stage of precipitation.

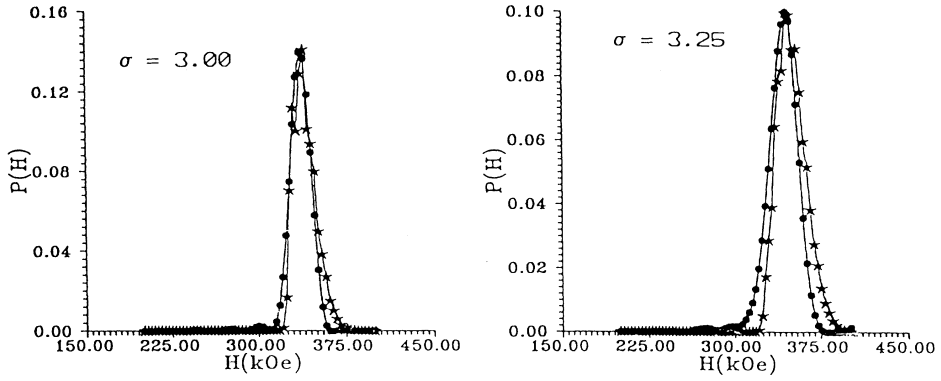

(a) (b)

FIG. 1. Theoretical * and experimental ● hyperfine field distribution $P(H)$ obtained with $\Delta H_{\mathrm{Ni},i}$ from Ref. 4 for (a) sample *A* and (b) sample *C*.

A. $Fe_{1-x}Ni_x$ alloys

The experimental mean hyperfine field $\overline{H}_{\mathrm{expt}}$ and isomer shift $\overline{\delta}_{\mathrm{expt}}$ corresponding to the arithmetic mean of the experimental values assigned to the various individual sites are, for all samples, in perfect agreement with the experimental values reported previously.[9,10] This signifies that the experimental hyperfine field distributions related to our samples are correctly defined. However, with the Ni increments, $\Delta H_{\mathrm{Ni},1}=9.4$ kOe and $\Delta H_{\mathrm{Ni},2}=7$ kOe,[4] a systematic disagreement with the mean calculated hyperfine field values given by the binomial law is observed over all x contents. We did not suspect the binomial law, as the good homogeneity of our sample was demonstrated by the x-ray microprobe analysis. On the other hand, at this step, the $\overline{H}_c$ calculation of the mean MHF by the binomial law was performed with the known $\Delta H_{k,i}$ increments involving only the two first coordination shells. Consequently, the requirement of the upper shell contributions appeared obvious. The $P(H)_c$ curves obtained from relation (6) which, then, takes into account their contributions via the width σ of the Gaussian function, did not give any greater agreement, however, regardless of the σ value. Figure 1 presents the comparison between $P(H)_c$ and $P(H)_{\mathrm{expt}}$ for samples *A* and *C* for the smallest *R* value with σ, respectively, equal to 3 and 3.25 kOe and with the above $\Delta H_{\mathrm{Ni},i}$ increments. We remark that the shift still remains. A significantly better fit of $P(H)_c$ and $P(H)_{\mathrm{expt}}$ was found for other precise values of $\Delta H_{\mathrm{Ni},1}$, $\Delta H_{\mathrm{Ni},2}$, and σ (Fig. 2). It appears that, within the experimental composition limits, the available $\Delta H_{\mathrm{Ni},1}$ and $\Delta H_{\mathrm{Ni},2}$ increments can be regarded as constant with x and equal, respectively, to 6.1 ± 0.5 and 4.4 ± 0.5 kOe. The σ value increases logically with x from 6.0 to 8.7 kOe, as it reflects the effect of all solute neighbors without limitation of the shell distance (Table II). However, a specific value of the $\Delta H_{\mathrm{Ni},i}$ increments for each individual upper shell, which could include the fifth upper shell, has no physical meaning, bearing in mind the magnitudes of $\Delta H_{\mathrm{Ni},1}$, $\Delta H_{\mathrm{Ni},2}$ and σ. Nevertheless, σ is of the same order as the $\Delta H_{\mathrm{Ni},1}$ and $\Delta H_{\mathrm{Ni},2}$ values. This reflects the common picture of the Ni impurity represented by delocalized potentials. We can

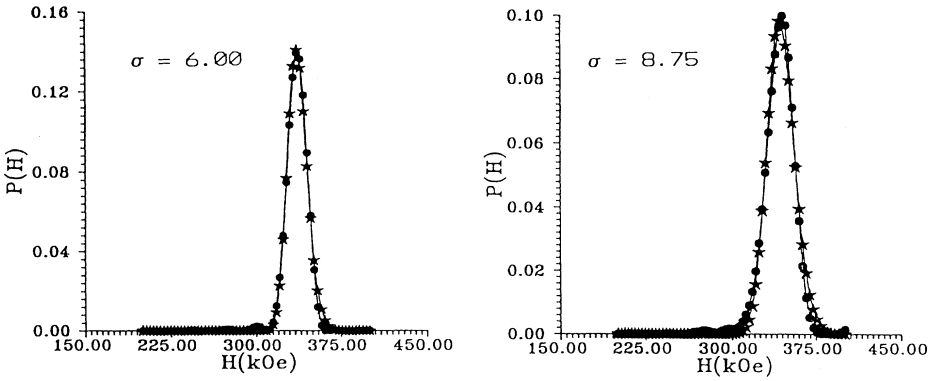

(a) (b)

FIG. 2. Theoretical * and experimental ● hyperfine field distribution $P(H)$ obtained with $\Delta H_{\mathrm{Ni},1}=6.1$ kOe and $\Delta H_{\mathrm{Ni},2}=4.4$ kOe for (a) samples *A* and (b) sample *C*.

TABLE II. Field increments and σ values corresponding to R_{min} for Fe-Ni samples. L is the composition limit. The respective accuracy for σ, $\bar{H}_{expt}$ and $\bar{\delta}$ is ± 0.25, ± 1, and ± 0.005.

Sample	L	ΔH_1 (kOe)	ΔH_2 (kOe)	σ (kOe)	$\bar{H}_{expt}$ (kOe)	$\bar{\delta}$ (mm/s)
A	0.176	6.6	4.8	8.7	342.5	0.035
A	0.180	6.4	4.8	8.7	342.5	0.035
B	0.119	5.9	4.3	6.2	338.5	0.032
B	0.123	5.6	3.9	6.2	338.5	0.032
C	0.090	6.6	4.8	6.0	338.3	0.031
C	0.094	6.4	4.8	6.0	338.3	0.031

conclude that the additivity model is fully obeyed up to $x = 0.18$ Ni.

B. Ternary alloys in their initial stage

1. Fe-Ni-W

From the previous analysis of the field increments in dilute binary alloys, the respective effects of Mo (4*d* solute) and W (5*d* solute) were found to be the most important.[4] The preliminary study of Fe-Ni-W alloys with low W concentration was of particular interest to check the perturbation caused by a third element in the Ni $\Delta H_{k,i}$ increments and could confirm the results obtained in the case of the Mo addition. The homogeneity of the alloys detected by x-ray microanalysis authorized the assumption of a statistical distribution of the solutes. The Mössbauer spectra of the two quenched samples (80 °C/s and 300 °C/h) show the typical satellites relevant to W substitution. As an example, on Fig. 3 the spectrum of the sample quenched at the rate of 80 °C/s is reported. $P(H)_c$ calculated with the known field increments $\Delta H_{k,i}$, where $i = 1,2$ and $k =$ Ni,W ($+9.4$ and $+7$ kOe for Ni, -45.8 and -24.7 kOe for W) does not reproduce the experimental results (Fig. 4). A preliminary evaluation by the discrete site procedure, considering the alloy as a pseudobinary Fe-Ni alloy substituted by 3.0 at. % W, confirmed this discrepancy so that the previously determined values for Ni could not alone be responsible for this fact. The W coefficients, being ten times larger than those of Ni, must also suspected in this light. Whatever the quenching rate, the available field increments are, respectively, for $\Delta H_{Ni,1}, \Delta H_{Ni,2}, \Delta H_{W,1}$, and $\Delta H_{W,2}$ equal to 5.3 ± 0.7, $+3.3 \pm 0.7$, -53.0 ± 1.0, and -29.7 ± 1.0 kOe. The σ value of 9 kOe compared to the W field increments shows the preponderance of the first two coordination shells for the ^{57}Fe perturbations caused by W and hence the localized effect of W.

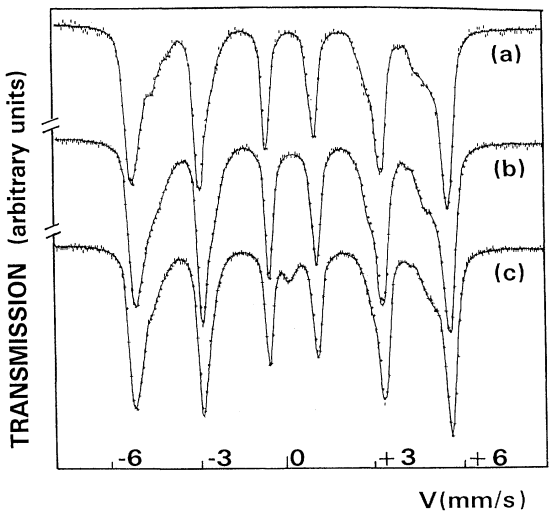

FIG. 3. Mössbauer spectra at room temperature for (a) Fe-Ni-W (I) quenched at the rate of 80 °C/s, (b) Fe-Ni-Mo_3 (II) quenched at the rate of 300 °C/h, and (c) Fe-Ni-Mo_3 (II) aged 72 h at 450 °C.

2. Fe-Ni-Mo

Noticeable disparities appear in the behavior of the quenched Fe-Ni-Mo_3 (II) and Fe-Ni-Mo_5 (III) alloys (Figs. 3 and 5). Whatever is the quenching rate, no paramagnetic line is revealed in the Mössbauer spectra of sample II. In contrast, a central line with $\delta = 0.040 \pm 0.005$ mm/s is observed for the sample III spectra, even after a cooling down to 77 K. Its amplitude of 0.5%, for the 80 °C/s quenching rate, increases up to 1.3% for the 300 °C/h cooling rate. After an aging duration of 1 h at 450 °C, the paramagnetic peak vanishes. Consequently, it does not result from the presence of residual austenite. Moreover, after cooling down to liquid nitrogen temperature, it should disappear, something which is not observed. The paramagnetic line for 80 °C/s and 300 °C/h cooling rates is then relevant to the occurrence of segregation phenomena of atoms within the martensite, which is more extensive when the cooling rate is slower. The bright field micrographs of the Fe-Ni-Mo_5 (III) samples cooled at the rate of 300 °C/h do not show any residual austenite either at the interfaces or inside the martensite laths and no precipitate of the type discussed below is detected (Fig. 6). These remarks give evidence for the fact that the paramagnetic line observed in the Mössbauer spectra may result from some segregation of atoms in the grain, known as Cottrell clouds.

However, in order to remove any ambiguity about the analysis of the hyperfine field distribution, we focused our attention more particularly on the sample free from any paramagnetic line. On the basis of this remark and the TEM observations, we considered the following alloys as being in the initial stage of the precipitation process: Fe-Ni-Mo_3 (II) quenched at the rates of 80 °C/s and 300 °C/h

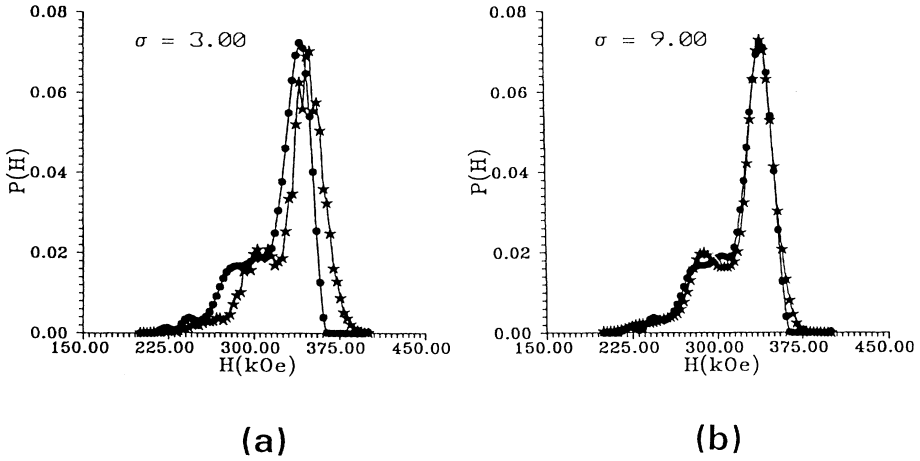

FIG. 4. Theoretical * and experimental ● hyperfine field distribution $P(H)$ for Fe-Ni-W (I) calculated with (a) $\Delta H_{\mathrm{Ni},i}$, $\Delta H_{\mathrm{W},i}$ given in Ref. 4 and (b) $\Delta H_{\mathrm{Ni},1} = 5.3 \pm 0.7$ kOe, $\Delta H_{\mathrm{Ni},2} = 3.3 \pm 0.7$ kOe, $\Delta H_{\mathrm{W},1} = -53.0 \pm 1.0$ kOe, and $\Delta H_{\mathrm{W},2} = -29.7 \pm 1.0$ kOe.

and Fe-Ni-Mo_5 (III) aged for 1 h at 450 °C (see Table III). For these alloys, the hyperfine field distributions were obtained with δ, ϵ, and H correlations similar to those of sample I, on the assumption of a statistical distribution of solutes, within the composition limits given by the x-ray microprobe analysis. Nevertheless, for all these alloys, the $P(H)_c$ distribution calculated with the field increment values available up to now[4] was shifted towards high fields.

As an example, the case of Fe-Ni-Mo_3 (II) cooled at the rate of 300 °C/h is presented on Fig. 7. It suggests that the Ni field increments are too large and the Mo increments too small ($\Delta H_{\mathrm{Mo},1} = -38.7$ and $\Delta H_{\mathrm{Mo},2} = -31.6$). The best simulation for sample II is then given with the modified values $\Delta H_{\mathrm{Ni},1}$ and $\Delta H_{\mathrm{Ni},2}$, respectively, equal to 5.3 ± 0.7 and 3.3 ± 0.7 kOe, and $\Delta H_{\mathrm{Mo},1}$ and $\Delta H_{\mathrm{Mo},2}$, respectively, equal to -49.5 ± 1.0 and -24.7 ± 1.0 kOe, providing evidence for a differentiation between the effects of the first and second neighboring shells, with Ni and Mo content equal, respectively, to 18.3 and 3.4 at. %, in perfect agreement with the x-ray microanalysis. The Ni coefficients remain, within the experimental accuracy, in the range of values obtained for the Fe-Ni and Fe-Ni-W alloys found on the above binary alloys. The Mo values, lower than those of W, are in agreement with the sequence of the field increment magnitudes identified previously.[4] The σ value, accounting for the upper shells, expresses the localized effect of Mo. The constancy of $\Delta H_{k,1}$ and $\Delta H_{k,2}$ increments for the two Mo contents attests also to the validity of the additivity model and the random atomic distribution in the matrix for this composition range. Nevertheless, even in the case of sample II, the quality of the best simulation representative of $P(H)_{\mathrm{expt}}$ is directly affected by the thermal treatments undergone by the samples. R is smaller for the quenching rate of 300 °C/h. The slight oscillations around the theoretical curve appearing for the quenching rate of 80 °C/s vanish for 300 °C/h, indicating a homogenization of the matrix without Cottrell clouds, as one can expect from the fact that the molybdenum content is low.

In the case of sample III aged 1 h at 450 °C, the minimal R factor is obtained with the same $\Delta H_{k,i}$ increments as for sample II but with Ni and Mo contents equal to 15.0 and 5.7 at. %, respectively, within the accuracy given by the x-ray microanalysis (Fig. 8). One must

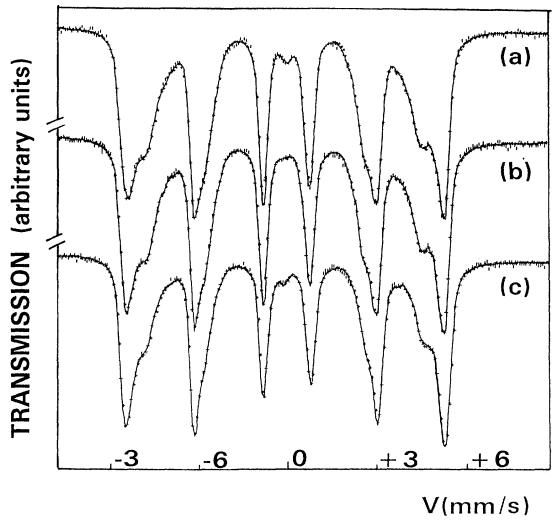

FIG. 5. Mössbauer spectra at room temperature for Fe-Ni-Mo_5 (III) sample (a) quenched at the rate of 300 °C/h, (b) aged at 450 °C for 1 h, and (c) aged at 450 °C for 72 h.

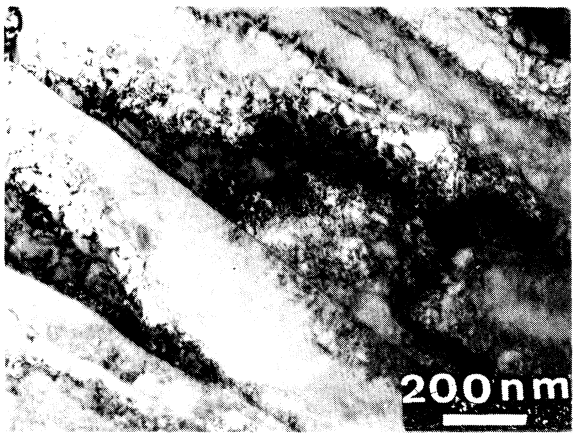

FIG. 6. Bright field micrographs for Fe-Ni-Mo_5 (III) cooled at the rate of 300 °C/h.

TABLE III. Coefficients and hyperfine parameters fitting the calculated hyperfine field distribution. M_R is the matrix composition minimizing the R factor, α_p the paramagnetic peak area in %, δ_p the paramagnetic peak isomer shift, and σ the variance of the Gaussian function in kOe. The respective accuracy for $\Delta H_{\mathrm{Ni},1}$, $\Delta H_{M,1}$, $\Delta H_{\mathrm{Ni},2}$, $\Delta H_{M,2}$, σ, $\overline{H}_{\mathrm{expt}}$, δ_p, and α_p is ± 0.7, ± 1, ± 0.7, ± 1, ± 0.25, ± 1, ± 0.005, and ± 0.2.

Alloy	Heat treatment	M_R	$\Delta H_{\mathrm{Ni},1}$	$\Delta H_{M,1}$	$\Delta H_{\mathrm{Ni},2}$	$\Delta_{M,2}$	σ	$\overline{H}_{\mathrm{expt}}$	δ_p	α_p
Fe-Ni-W_3	80 °C/s 300 °C/h	$Fe_{80.7}Ni_{16.3}W_{3.0}$	5.3	−53.0	3.3	−29.7	9	322		0
Fe-Ni-Mo_3	80 °C/s 300 °C/h	$Fe_{78.3}Ni_{18.3}Mo_{3.4}$	5.3	−49.5	3.3	−24.7	10.5	321		0
	Aged 72 h/450 °C	$Fe_{79.8}Ni_{17.8}Mo_{2.4}$	5.3	−49.5	3.3	−24.7	9.25	323	−0.077	3.4
Fe-Ni-Mo_5	Aged 1 h/450 °C	$Fe_{79.3}Ni_{15.0}Mo_{5.7}$	5.3	−49.5	3.3	−24.7	9	307		0
Fe-Ni-Mo_5	Aged 72 h/450 °C	$Fe_{81.5}Ni_{14.0}Mo_{4.5}$	5.3	−49.5	3.3	−24.7	8.5	315	−0.112	1.3

point out that the best R factor for sample III quenched at both rates of 80 °C/s and 300 °C/h is obtained, within the experimental uncertainties, with the same field increments and alloy composition, but its value is incorrect. The expansion is that the inhomogeneities which exist within the samples initiate a precipitation as Cottrell clouds already discussed above, for a quenching rate of 80 °C/s. A slower quenching rate favors, on the one hand, the emergence of new precipitates increasing the paramagnetic line amplitude and, on the other hand, a better homogenization of the matrix. The aging of one hour restores a better statistical distribution in the matrix concomitantly with the disappearance of the precipitates. Moreover, the σ value decreases from 10.25 to 9.00 kOe and gives evidence for a better definition of the local environment.

The information that can be drawn from the studies at room temperature of the ternary alloys $Fe_{1-x-y}Ni_xM_y$ (M = Mo,W) with low y value, in the initial stage, are that the field perturbations induced by the Ni atoms are additive and equal to those found in the binary Fe-Ni alloys within the limit of the experimental accuracy. Any attempt to refine this determination is illusive, owing to the small $\Delta H_{\mathrm{Ni},1}$ and $\Delta H_{\mathrm{Ni},2}$ values. The effect of W and Mo is more negative than that found in binary alloys, in agreement with the same trend mentioned for Cr in ter-

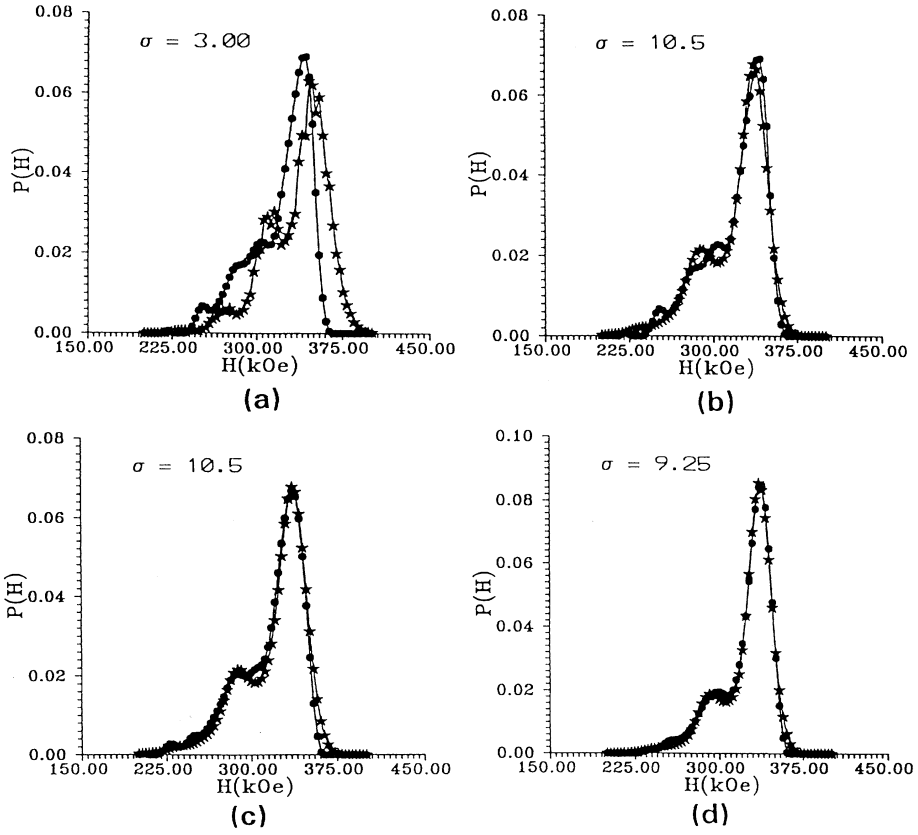

FIG. 7. Theoretical * and experimental ● hyperfine field distribution $P(H)$ for Fe-Ni-Mo_3 (sample II): (a) $\Delta H_{M,i}$ given in Ref. 4; (b), (c), and (d) $\Delta H_{\mathrm{Ni},1} = 5.3 \pm 0.7$ kOe, $\Delta H_{\mathrm{Ni},2} = 3.3 \pm 0.7$ kOe, $\Delta H_{\mathrm{Mo},1} = -49.5 \pm 1$ kOe, and $\Delta H_{\mathrm{Mo},2} = -24.7 \pm 1$ kOe; (b) coupling rate of 80 °C/s; (c) cooling rate of 300 °C/h; (d) sample aged 72 h at 450 °C.

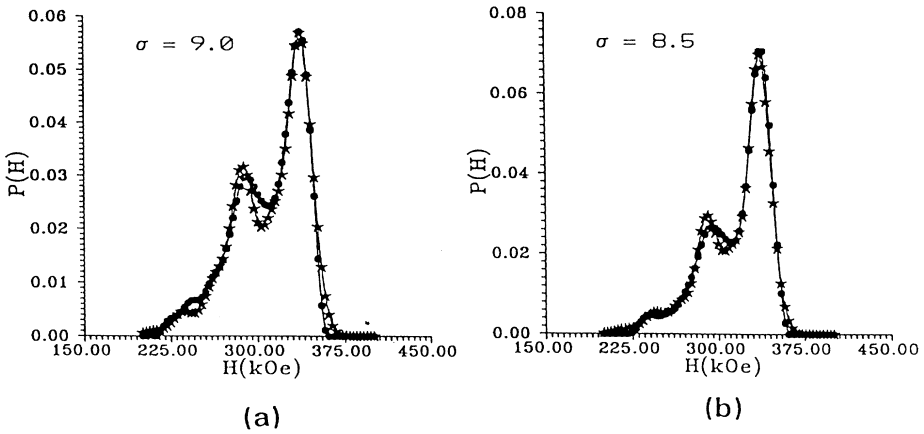

FIG. 8. Theoretical * and experimental ● hyperfine field distribution $P(H)$ for Fe-Ni-Mo_5 (sample III) with $\Delta H_{Ni,1} = 5.3 \pm 0.7$ kOe, $\Delta H_{Ni,2} = 3.3 \pm 0.7$ kOe, $\Delta H_{Mo,1} = -49.5$ kOe, and $\Delta H_{Mo,2} = -24.7$ kOe, (a) aging 1 h at 450 °C and (b) aging 72 h at 450 °C.

nary $Fe_{1-x-y}Ni_xCr_y$ alloys.[6] However, the additivity of the $\Delta H_{k,i}$ increments and the independence of the effect of Ni and Mo observed in these alloys demonstrate the possibility of Ni and Mo analysis in the $Fe_{1-x-y}Ni_xMo_y$ samples in the latest step of aging.

C. Ternary aged alloys

The Fe-Ni-Mo_3 (sample II) and Fe-Ni-Mo_5 (sample III) alloys aged 72 h at 450 °C are characterized by the highest hardness values.[11,12] Consequently, this aging duration was chosen for the Mössbauer spectroscopy studies and TEM experiments.

The Mössbauer spectrum of sample II shows a broad central paramagnetic line with a δ value and relative abundance α_p equal, respectively, to -0.077 ± 0.005 mm/s and $(3.4 \pm 0.2)\%$ (Fig. 3). The sample III spectrum is characterized by a weaker paramagnetic line $\delta = -0.112 \pm 0.005$ mm/s and $\alpha_p = (1.3 \pm 0.2)\%$ (Fig. 5). This suggests that the Fe amount in the precipitate is lower. The matrix hyperfine field distribution, extracted from the experimental data, has been reproduced with field increment values equal to those deduced from the initial-stage sample spectra, the Ni and Mo relative populations being adjusted.

The Fe content in the precipitate is defined from the area of the iron paramagnetic peak, which implies the remaining iron atom content in the matrix when one takes into account the initial iron atomic concentration in the alloy. On the other hand, the $P(H)_{expt}$ distribution of the aged matrix provides the Fe:Ni and Fe:Mo ratios in the matrix, leading to the number of Ni and Mo atoms involved in the precipitates.

Such analysis therefore leads accurately to the relative atomic Ni and Mo contributions to the matrix hyperfine field distribution. However, the number of Fe atoms involved respectively in the precipitates and in the matrix can only be deduced from knowledge of the relative Lamb-Mössbauer f factors. The possible assumptions about these values can be justified only by subsequent experiments with other methods. This is the reason for the subsequent TEM investigations.

The simple assumption of an f factor for the precipitate identical to that of the matrix leads to an atomic precipitate composition equal to $Fe_{50\pm5}Ni_{30\pm5}Mo_{20\pm5}$ for sample II and $Fe_{25\pm5}Ni_{40\pm5}Mo_{35\pm5}$ for sample III. From the ternary Fe-Ni-Mo diagram several combinations can explain the composition obtained for sample II precipitates: $(Fe\text{-}Ni)_4Mo$, $(Fe\text{-}Ni)_7Mo_2$, and $(Fe\text{-}Ni)_3Mo$ with, respectively, tetragonal $I4/m$, hexagonal $P6_3/mmc$, and orthorhombic $Pmmm$ space groups. The sample III precipitate overall composition close to the formula $(Fe\text{-}Ni)_2Mo$ could be interpreted as belonging to one form of the hexagonal $P6_3/mmc$ structure. In fact, great analogies appear in the TEM diffraction patterns of both samples. A careful analysis reveals two kinds of precipitates:

TABLE IV. Volume per atom (v_a) for the indexed species deduced from the unit cell volume and the number of atoms per unit cell (n).

Phase		Structure	Parameters (nm)	n	v_a (nm^3)
Ni_3Mo		orthorhombic	$a = 0.5064$		
			$b = 0.04224$	8	0.011893
			$c = 0.4448$		
ω	A_8B, A_7B_2	hexagonal			
		$c/a = 0.352$	$a = 0.704$	9	0.011827
	A_2B	hexagonal	$c = 0.248$		
		$c/a = 0.612$	$a = 0.4058$	3	0.011812
			$c = 0.2485$		
Martensite		bcc	$a = 0.278$	2	0.010742

the $(Fe\text{-}Ni)_3Mo$ phase (orthorhombic $Pmmm$) and the ordered ω phase $(Fe\text{-}Ni)_7Mo_2$ (hexagonal $P6_3/mmc$).

The observed diffraction pattern of Ni_3Mo with the $\langle 001 \rangle$ zone axis of the bcc martensitic matrix is presented in Fig. 9(a). The ω phase is revealed in the diffraction pattern of the martensite zone axes $\langle 110 \rangle$ and $\langle 113 \rangle$ where extra spots are present at the positions 1/3 and 2/3 in the reciprocal directions $\langle 112 \rangle^*$ [Fig. 9(b)], in agreement with the interfacial coherency given previously by Shimizu and Okamato.[13] Moreover, this ω phase is ordered because the forbidden spots $(10\bar{1}0)$ and $(20\bar{2}0)$ are present on the zone axis $\langle 111 \rangle$ of the martensite [Fig.

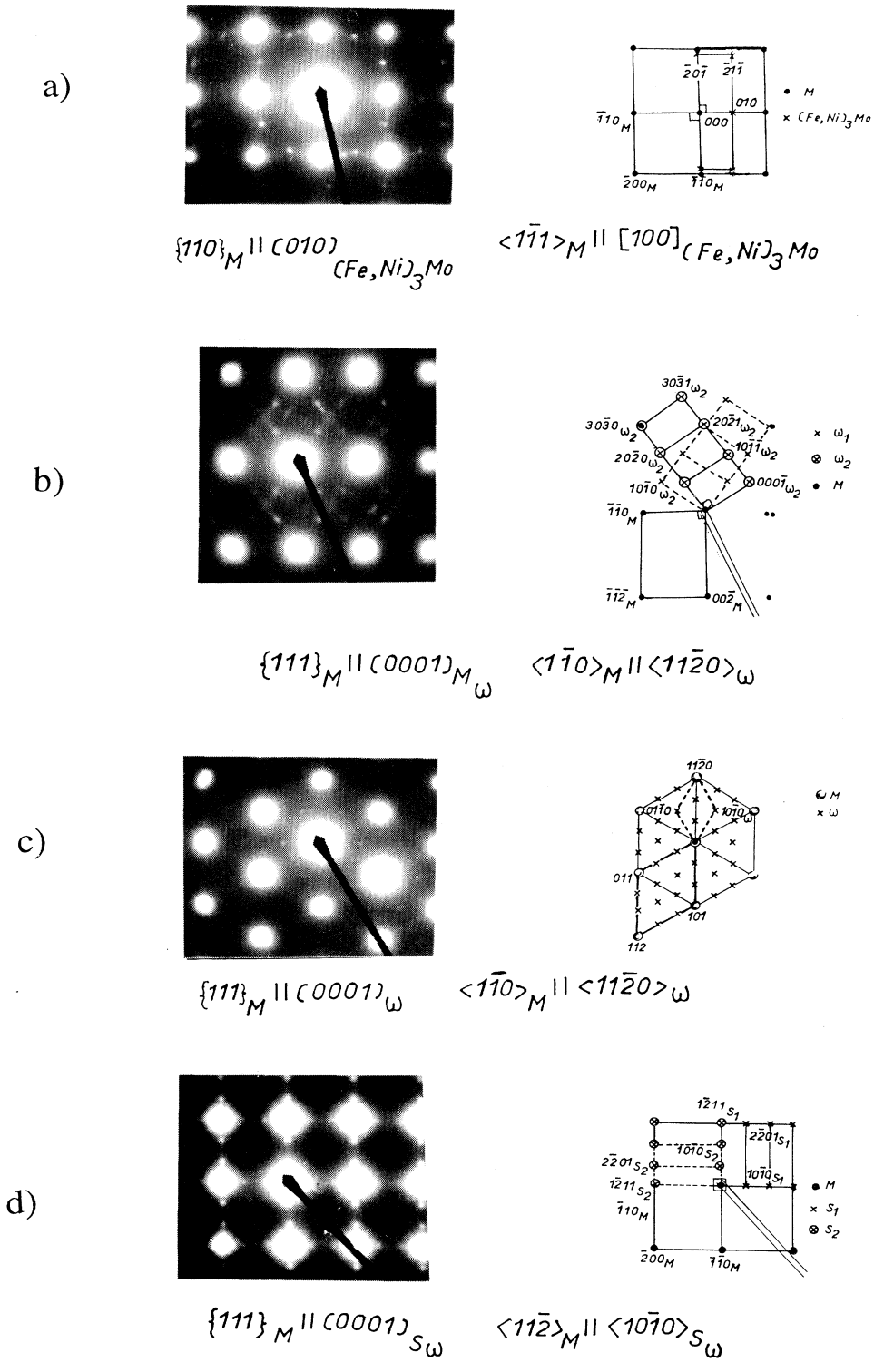

FIG. 9. Diffraction pattern of the precipitates after 72-h aging at 450 °C for $Fe\text{-}Ni\text{-}Mo_3$ (sample II): (a) Ni_3Mo on $\langle 001 \rangle$ zone axis of the bcc martensitic matrix; (b) ω phase on $\langle 110 \rangle$ zone axis of the bcc martensitic matrix showing the ω_1 and ω_2 variants; (c) ω phase on $\langle 111 \rangle$ zone axis of the bcc martensitic matrix showing the ordering of the phase; (d) ω phase on $\langle 001 \rangle$ zone axis of the bcc martensitic matrix showing its superstructure of A_7B_2 type.

9(c)]. In the diffraction pattern shown in Fig. 9(b), two different families ω_1 and ω_2 of the ω phase are present among the four possible resulting from the orientation relationship between ω and the bcc matrix. In addition, in the diffraction pattern showing the bcc martensite $\langle 001 \rangle$ zone axis [Fig. 9(d)], spots at the positions 1/3 and 2/3 of the reciprocal direction $\langle 110 \rangle^*$ belong to the ω superstructure of A_7B_2 type described by Yedneral and Perkas.[14] According to these authors, the ω phase evolves from $(Fe\text{-}Ni)_8Mo$ to $(Fe\text{-}Ni)_7Mo_2$ and finally $(Fe\text{-}Ni)_2Mo$ in relation to the nature of the occupied sites.

In the case of all the phases mentioned above, it is possible to relate their volume fractions to their atomic fractions, having in mind the unit cell parameters and their corresponding numbers of atoms (Table IV). The volume fraction of the precipitates evaluated from the TEM observation (5–10 %) (Fig. 10) is consistent with the small fraction of the various components Fe, Ni, and Mo involved in the precipitates deduced from the Mössbauer spectra (5%), supporting our hypothesis of similar f factors for the precipitates and for the matrix. Furthermore, the TEM micrographs lead to an evaluation of the volume ratio of the two phases (Ni_3Mo to ω) equal to 1 (Fig. 10).

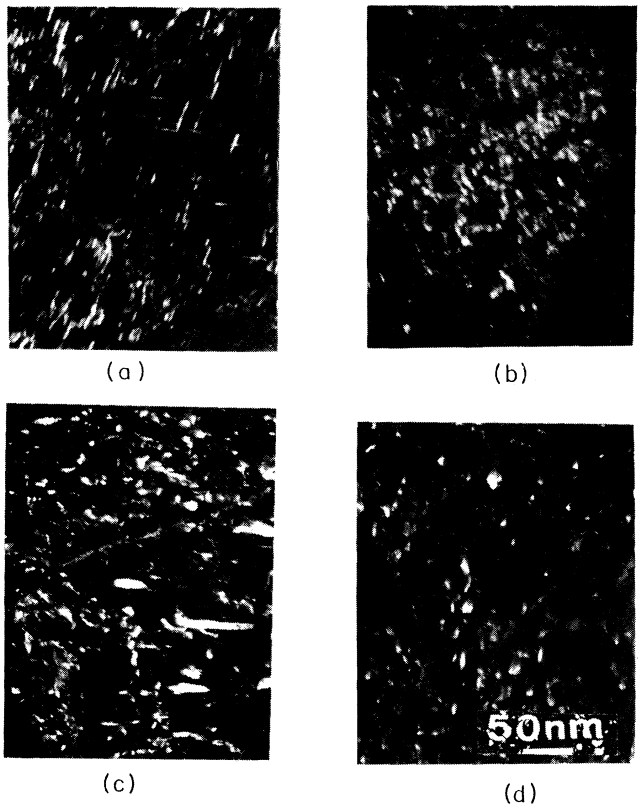

FIG. 10. Dark field of the precipitates after 72-h aging at 450 °C for Fe-Ni-Mo_3 (sample II): (a) Ni_3Mo intermetallic compound and (b) ω phase for Fe-Ni-Mo_5. (Sample III): (c) Ni_3Mo intermetallic compound and (d) ω phase.

It happens that, with the TEM information of the volume ratio of the Ni_3Mo and ω phases and the assumption of the f factor equality, corroborated by the small volume fraction of the precipitates observed by TEM, it is possible to deduce the precipitate composition. The only restriction about this evaluation is the distribution of the Fe and Ni atoms among both phases $(FeNi)_3Mo$ and ω-$(FeNi)_7Mo_2$ as it is not possible to distinguish from the Mössbauer spectrum the two paramagnetic precipitate species.

It must be emphasized that the two samples $Fe_{78.3}Ni_{18.3}Mo_{3.4}$ and $Fe_{79.3}Ni_{15.0}Mo_{5.7}$ lie in the limiting range of coherent precipitation of the A_7B_2 superstructure[16] but the (Fe,Ni) to Mo ratio is lowered for $Fe_{79.3}Ni_{15.0}Mo_{5.7}$. Nevertheless, the ω phase evolves to its limit form of $(FeNi)_2Mo$ type .[15]

V. CONCLUSION

On the basis of the good homogeneity of our samples exhibited by x-ray microanalysis, we have been able to explain the magnetic field perturbations experienced by a ^{57}Fe nucleus surrounded by Ni atoms, in binary $Fe_{1-x}Ni_x$ alloys up to 18 at. % Ni with the model of additivity of the solute influences on the assumption of a statistical atomic distribution. There seems no evidence for departure from this model at room temperature in the case of the ternary $Fe_{1-x-y}Ni_xM_y$ alloys, in the composition range $x \simeq 0.15-0.18$, $y \simeq 0.03-0.05$ (M =W,Mo).

Aging phenomena in ternary bcc ferromagnetic systems (Fe-$M-M'$) can be elucidated by understanding of the matrix modifications as well as the concomitant precipitate evolution. However, the analysis of such $P(H)$ profiles is subordinated to systematic checking of the validity of the additivity model and a determination of the field increments $\Delta H_{k,i}$ measured on reference alloys, around the explored compositions.

With such an approach, an accurate determination of the relative M and M' matrix depletion can be performed, although the resonant atom is ^{57}Fe. When the Lamb-Mössbauer factor of the precipitates is not known, which is the case for many phases, TEM experiments, as illustrated above, give support for the conversion of the resonant fractions into atomic fractions.

In the case of the $Fe_{78.3}Ni_{18.3}Mo_{3.4}$ and $Fe_{79.3}Ni_{15.0}Mo_{5.7}$ alloys studied here, we have been able, by the complementarity of Mössbauer spectroscopy and transmission electron microscopy, to detect small volume fractions of precipitates, and give a rather complete description for them. Our assumption of identical f factors for the matrix and precipitates, corroborated by the TEM experiments, allowed us to define the overall composition of the precipitated part. The main result is the presence, in all cases, of two metastable phases: $(Fe_{(1-x)}Ni_x)_3Mo$ and $\omega(Fe_{(1-y)}Ni_y)_7Mo_2$ with an overall Fe to (Ni,Mo) atomic ratio given by Mössbauer spectroscopy as being about twice as small for the sample with the highest Mo content as for that with the lowest. This fact indicates that the ω phase tends to its limiting form $(Fe\text{-}Ni)_2Mo$.

*Also at Institut Universitaire de Formation des Maîtres de l'Académie de Créteil, 94388 Bonneuil, France.
[1]W. Sha, D. Phil., University of Oxford, 1991.
[2]C. Servant, O. Lyon, and J. P. Simon, Acta Metall. **37**, 2403 (1989).
[3]B. Fultz, A. Hamdet, and D. H. Pearson, Acta Metall. **37**, 2841 (1989).
[4]I. Vincze and I. A. Campbell, J. Phys. F **3**, 647 (1973).
[5]B. Fultz and J. W. Morris, Phys. Rev. B **34**, 4480 (1986).
[6]S. Nagy, E. Kuzmann, A. Vertes, G. Szabo, and G. Konozos, Nucl. Instrum. Methods Phys. Res. Sect. B **34**, 217 (1988).
[7]J. L. Dormann, L. Brossard, and G. A. Fatseas, Phys. Status Solidi B **52**, K23 (1972).
[8]G. Le Caer and J. M. Dubois, J. Phys. E **12**, 1083 (1979).
[9]G. K. Wertheim, V. Jaccarino, J. H. Wernick, and D. N. E. Buchanan, Phys. Rev. Lett. **12**, 24 (1964).
[10]I. Vincze, I. A. Campbell, and A. J. Mayer, Solid State Commun. **15**, 1495 (1974).
[11]A. Agnel, F. Hedin, G. Maeder, C. Servant, and P. Lacombe, Acta Metall. **25**, 1445 (1977).
[12]R. Courrier and G. Le Caer, Mem. Sci. Rev. Metall. **71**, 691 (1974).
[13]K. Shimizu and H. Okamato, J. Jpn. Inst. Met. **35**, 204 (1971).
[14]A. F. Yedneral and M. D. Perkas, Fiz. Met. Metall. **33**, 315 (1972).
[15]N. Bouzid, C. Servant, and O. Lyon, Philos. Mag. B **57**, 343 (1988).
[16]J. Bourgeot, Ph. Maitrepierre, J. Manenc, and B. Thomas, Mem. Sci. Rev. Metall. **67**, 125 (1970).

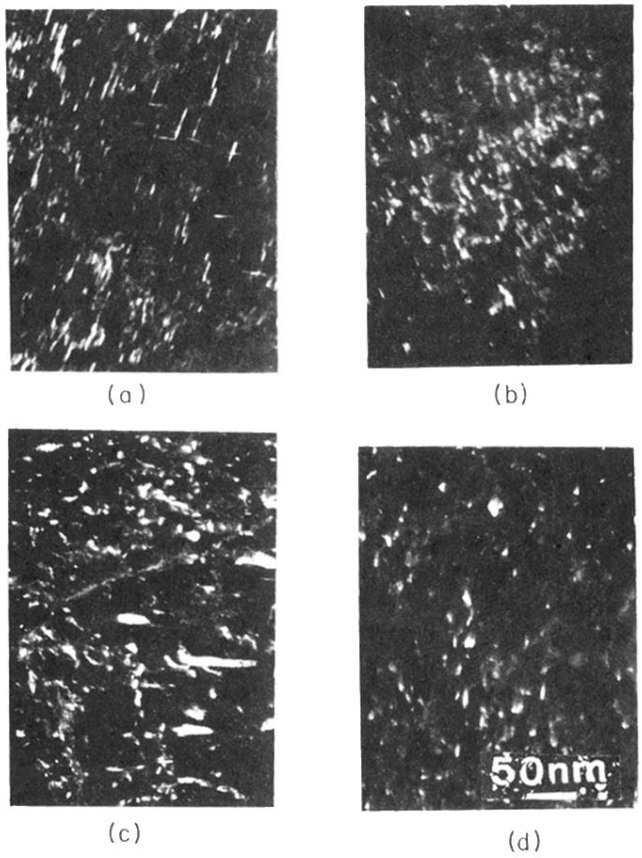

FIG. 10. Dark field of the precipitates after 72-h aging at 450 °C for Fe-Ni-Mo_3 (sample II): (a) Ni_3Mo intermetallic compound and (b) ω phase for Fe-Ni-Mo_5. (Sample III): (c) Ni_3Mo intermetallic compound and (d) ω phase.

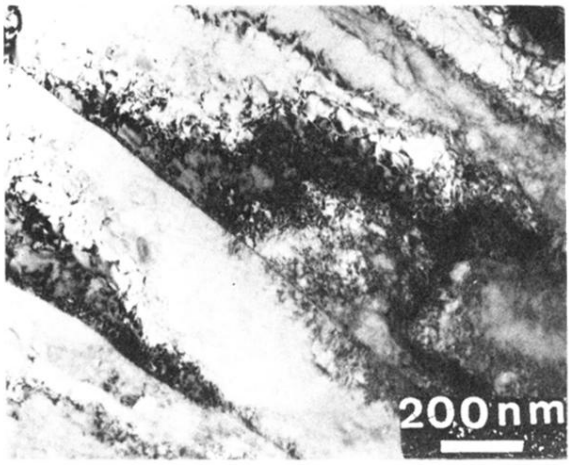

FIG. 6. Bright field micrographs for Fe-Ni-Mo_5 (III) cooled at the rate of 300 °C/h.

a)

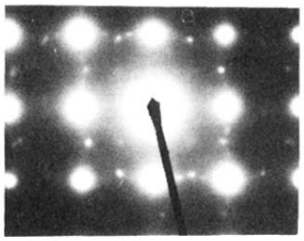

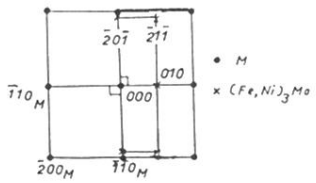

$\{110\}_M \parallel (010)_{(Fe,Ni)_3Mo}$ $\langle 1\bar{1}1\rangle_M \parallel [100]_{(Fe,Ni)_3Mo}$

b)

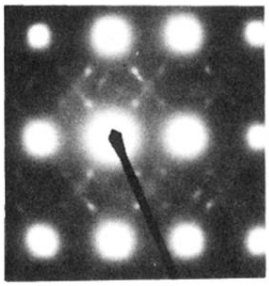

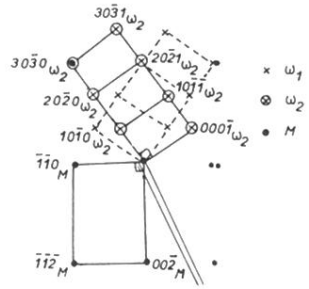

$\{111\}_M \parallel (0001)_{M_\omega}$ $\langle 1\bar{1}0\rangle_M \parallel \langle 11\bar{2}0\rangle_\omega$

c)

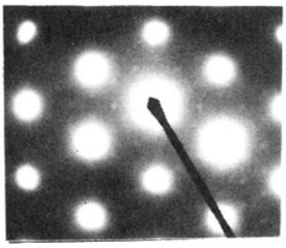

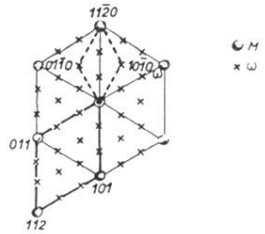

$\{111\}_M \parallel (0001)_\omega$ $\langle 1\bar{1}0\rangle_M \parallel \langle 11\bar{2}0\rangle_\omega$

d)

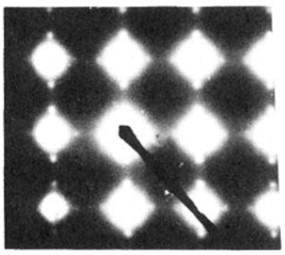

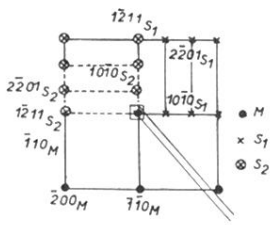

$\{111\}_M \parallel (0001)_{S_\omega}$ $\langle 11\bar{2}\rangle_M \parallel \langle 10\bar{1}0\rangle_{S_\omega}$

FIG. 9. Diffraction pattern of the precipitates after 72-h aging at 450 °C for Fe-Ni-Mo_3 (sample II): (a) Ni_3Mo on ⟨001⟩ zone axis of the bcc martensitic matrix; (b) ω phase on ⟨110⟩ zone axis of the bcc martensitic matrix showing the ω_1 and ω_2 variants; (c) ω phase on ⟨111⟩ zone axis of the bcc martensitic matrix showing the ordering of the phase; (d) ω phase on ⟨001⟩ zone axis of the bcc martensitic matrix showing its superstructure of A_7B_2 type.